Iraqi Journal for Computer Science and Mathematics

Manuscript 1277

Enhanced Detection of Intracranial Hemorrhage: A New Hybrid Model Design based on the U-Net Segmentation Method

Hassan F. Hassan

Hadeel K. Aljobouri

Oktay Algin

IRAQI JOURNAL FOR COMPUTER SCIENCE AND MATHEMATICS 2025;6:41–49

ORIGINAL STUDY

Enhanced Detection of Intracranial Hemorrhage: A New Hybrid Model Design based on the U-Net Segmentation Method

Hassan F. Hassan [a], **Hadeel K. Aljobouri** [a,*], **Oktay Algin** [b]

[a] Biomedical Engineering Department, College of Engineering, Al-Nahrain University, Baghdad, Iraq
[b] Interventional MR Clinical R&D Institute, Ankara University, Ankara 06100, Turkiye

ABSTRACT

Intracranial hemorrhage (ICH) denotes bleeding inside the skull, which can occur in or around the brain. Computed tomography (CT) has been used to detect ICH due to its high efficiency and accuracy. Nowadays, deep learning model design is introduced to allow an accurate and efficient classification of ICH in CT images. This work focused on developing U-Net-based models for the segmenting of ICH. Furthermore, the proposed model employed two transfer learning models, MobileNet and Xception, as the backbones of the U-Net topology. This approach aims to establish metrics that improve ICH treatment through precise segmentation techniques. A free dataset from the Radiological Society of North America (RSNA) was fed to the proposed model. This dataset comprises 5996 annotated CT images divided into four groups, with 1499 images per group. Three of these groups are for hemorrhage, and one is for the normal group. The average detection accuracy rates were impressive, with Intraparenchymal Hemorrhage (IPH) at 98%, Intraventricular Hemorrhage (IVH) at 98%, and Subdural Hemorrhage (SDH) achieving accuracy of 97%. This approach could assist radiologists in overloaded medical centers in precisely detecting ICH, especially in the local healthcare centers.

Keywords: Brain hemorrhages, Computer-aided diagnosis, Data analysis, Deep learning, Medical imaging

1. Introduction

Intracranial hemorrhage implies the existence of blood in the skull located above the cerebellum or cerebellar tonsils. Intracranial hemorrhages are generally divided into five categories: intraparenchymal, subdural, epidural, subarachnoid, and intraventricular, based on anatomical criteria (the involved part of the skull where blood is located) [1]. The three studied types are inside the skull: intraparenchymal, subdural, and intraventricular. In general, these types are included under the more general diagnosis of "cerebral hemorrhage" [2, 3]. Traumatic intracranial hemorrhages have been increasing substantially, and they require urgent medical attention [4, 5]. Prompt recognition of a brain tumor is crucial for patient care because evaluating brain tumor images is time-consuming and requires significant effort from radiologists [6]. The advanced imaging modalities to the current therapeutic paradigms include a focus on advanced 3D and 4D modalities, perfusion imaging, diffusion tensor imaging, magnetic resonance imaging, susceptibility-weighted imaging, and susceptibility mapping [7–9]. Experts in biomedical applications can analyze medical images tailored to specific medical purposes by employing various image-processing techniques [10]. Image processing is vital in diagnosing medical conditions. Treating brain tumors is difficult because of their intricacy. Recent advancements have led to new methods for identifying brain lesions, emphasizing the need for more inquiry into tumor extraction techniques [11].

Received 10 March 2025; revised 23 May 2025; accepted 2 June 2025.
Available online 2 July 2025

* Corresponding author.
E-mail addresses: hfhfhassan120@gmail.com (H. F. Hassan), hadeel_bme77@yahoo.com (H. K. Aljobouri), oktay.algin@umram.bilkent.edu.tr (O. Align).

https://doi.org/10.52866/2788-7421.1277

Neuroscience scientists have long been interested in medical image segmentation [12–14]. On the other hand, manual segmentation is a time-consuming job that necessitates the use of experienced professionals, so various semi-automatic review segmentation methods have been used, including region expansion and shrinking, as well as region competition and graph-cutting [15, 16]. Initially, low soft-tissue contrast and the pathology's tiny size made segmentation more difficult [17, 18]. Machine learning is a crucial field of artificial intelligence that involves algorithms and models that enable systems to perform tasks via pattern recognition and data analysis. Effective methods were used to extract insights from various imaging modalities [19, 20]. According to scholars, convolutional neural networks have advanced and are increasingly being used to adequately tackle these challenges that deal with the commonly expanded domain [18, 21, 22]. MobileNet and Xception were selected as encoder backbones due to their proven effectiveness in various medical imaging tasks. MobileNet, with its lightweight architecture and depthwise separable convolutions, has shown strong performance in diagnostic tasks such as COVID-19 and skin cancer detection [23]. Xception has also been widely adopted in medical image classification, including lung infection detection and histopathological analysis, due to its efficient representation learning [24].

1.1. Study significance

This work focused on the buildout and evaluation of three scenarios of deep learning models: U-Net, U-Net combined with MobileNet, and U-Net combined with Xception. The objective was to classify three types of intracranial hemorrhages, IPH, IVH, and SDH, with normal images. All models underwent training and testing on labeled datasets, and their performance was evaluated utilizing key parameters such as accuracy, recall, precision, and F1 score.

Although U-Net with pre-trained backbones such as MobileNet and Xception has been employed in various medical imaging tasks, to our knowledge, a direct comparative study focusing on their effectiveness in the segmentation and subsequent classification of specific ICH subtypes (IPH, IVH, SDH) from CT images remains limited. Furthermore, our proposed pipeline, where segmentation outputs are used to infer classification, offers a dual advantage of localizing hemorrhagic regions while supporting decision-level classification. This "segmentation-to-classification" design provides an interpretable and efficient alternative to conventional end-to-end classification models, especially when working with datasets where pixel-level masks are available or can be generated with reasonable effort.

2. Literature review

In (2020), Guo and his team studied 1,176 head CT scans, introducing ICHNet, a fully convolutional network for classifying and segmenting intracranial hemorrhage. While ICHNet showed improved performance over baseline models, it focused on a unified model rather than comparing backbone architectures [25]. In (2020), Lewicki et al. employed the ResNet-50 model to identify cerebral bleeding. A large dataset of 752,803 DICOM pictures was used, and achieved a high accuracy of 93.3% [26]. However, their approach was based on image-level classification and did not incorporate pixel-level segmentation or hybrid U-Net architectures. In (2021), Rava et al. investigated the efficacy of Canon's AUTO Stroke Solution in identifying cerebral hemorrhage, reporting 93% specificity and sensitivity based on data from 302 patients. Though promising, their system is proprietary, and its internal model structure was not made public, limiting reproducibility and benchmarking [27]. Wang et al. in (2021) used a 2D CNN and sequence models to detect cerebral hemorrhage in over 25,000 head CT images, achieving high AUCs. However, their method did not explore segmentation-based frameworks or the use of lightweight, computationally efficient architectures [28]. In (2023), Arman et al. used Bayesian Optimization to classify 1,074,271 photos into hemorrhage categories using a DenseNet model. While they evaluated the impact of optimization strategies, their study focused on classification only and did not explore segmentation-based approaches or hybrid models such as U-Net with transfer learning backbones [29].

3. Methodology

The workflow of the suggested framework is illustrated in Fig. 1. This section has three major parts: data preparation, preprocessing steps, and deep learning model design. The specifics of these sections will be explained in subsequent paragraphs.

3.1. Dataset

To conduct effective work, the needed data came from the RSNA Intracranial Hemorrhage dataset [30], which offers the quality annotations necessary for precise model training. The overall dataset contains 5996 labeled CT images, equally distributed among

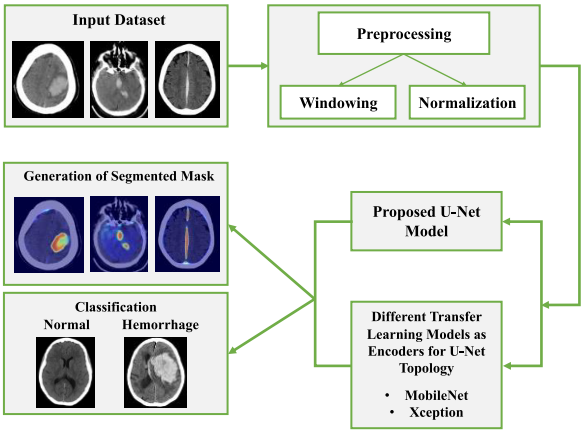

Fig. 1. Suggested workflow.

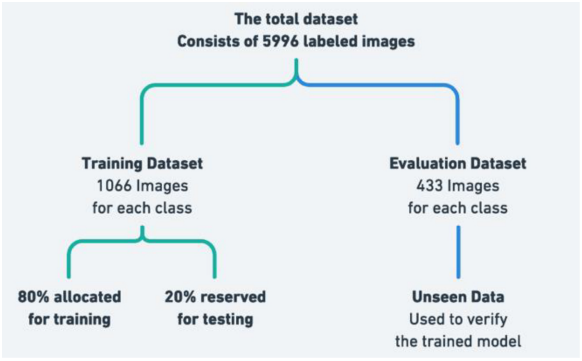

Fig. 2. Data partitioning workflow.

four hemorrhage classes (1499 images per class). The data was segregated between training and evaluation datasets in such a manner that for each case, 1066 and 433 images were used for training and evaluation, respectively. From the 1066 training images per class, 80% were allocated for training and 20% reserved for testing, resulting in a stratified 80/20 split, with no data augmentation applied. Fig. 2 exhibits the workflow of splitting the datasets.

3.2. Preprocessing

The original imaging data was obtained in Digital Imaging and Communications in Medicine (DICOM) format, the standard medical imaging format. To facilitate annotation using the Visual Geometry Group Image Annotator (VIA) tool, where the ground truth masks were manually created, the DICOM files were converted into the Portable Network Graphics (PNG) format. This conversion ensures compatibility with the annotation tool while preserving the necessary image quality for subsequent processing and analysis. The manipulation of image properties in medical imaging is facilitated through specific parameters,

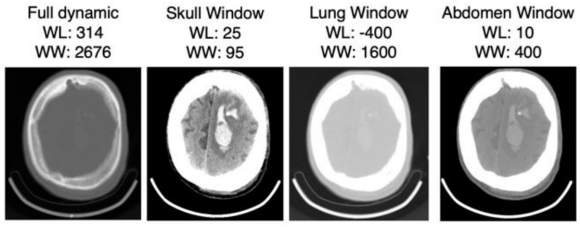

Fig. 3. Preprocessing for the CT image using different windows.

including Window Level (WL) and Window Width (WW). The WL serves a critical role in regulating the image's brightness, wherein an increase in WL results in a darker image, and a decrease in WL yields a brighter representation. Conversely, the WW is instrumental in determining the range of Hounsfield Unit (HU) values rendered visible in the image. An expanded WW permits a broader spectrum of detectable intensities, albeit at the expense of contrast. At the same time, a more constricted WW enhances image contrast but simultaneously narrows the visible intensity range.

Additionally, the Window Center is a key parameter defining the central intensity value within the presented grayscale window, influencing the overall perception of the image's tonal characteristics. The brain window, with a WW of 80 HU and a WL of 40 HU, was used to maximize the visualization of brain parenchyma details. Fig. 3 shows some of the different window effects.

3.3. The proposed models

U-Net is a fully convolutional deep learning architecture featuring a contracting path (Encoder) that captures context and an expansive path (Decoder) that brings this information to a full-resolution segmentation. It is constructed as an encoder-decoder architecture consisting of cascaded steps of 3×3 convolutions and rectified linear unit (ReLU) activation functions. Max-pooling operations are incorporated throughout the encoder portion of the network to reduce the feature maps into a lower-dimensional representation progressively. The decoder portion of the network then inverses the operations coherently with the encoder, upsampling the feature maps to match the original size of the input. It performs 2×2 transposed convolutions, or deconvolutions, channel expansion, and convolution operations. Skip connections reinforce the decoder networks by concatenating feature maps of the same size with feature maps from the contracting pathway. Fig. 4 shows the proposed U-net model architecture.

Transfer learning was employed to enhance feature extraction in the U-Net architecture. Two pre-trained

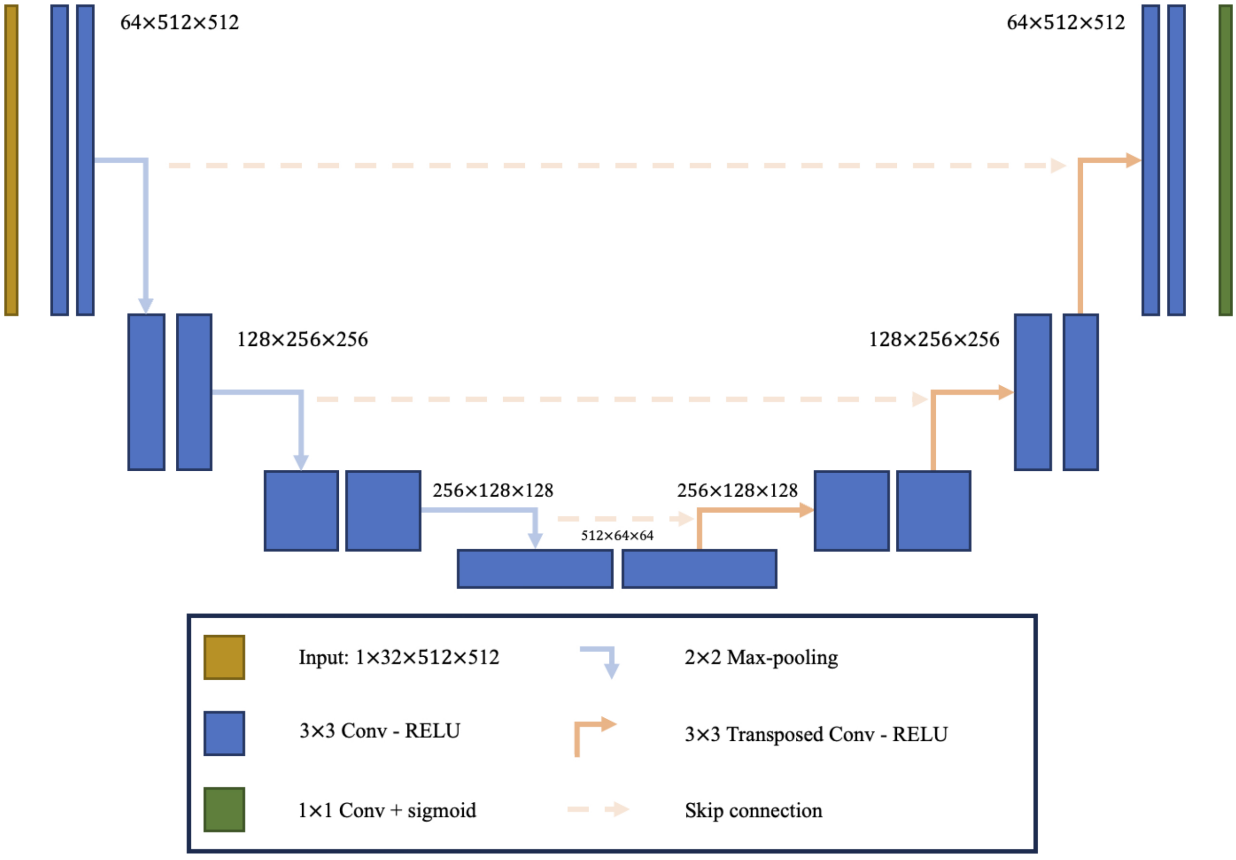

Fig. 4. Architecture diagram for the proposed 2D U-net model.

models—MobileNet and Xception—were used as encoders by removing their top classification layers and retaining the convolutional base initialized with ImageNet weights. A 1 × 1 convolution was applied to convert grayscale CT inputs into a 3-channel format compatible with these backbones. The final convolutional output from each encoder was passed to a custom decoder composed of upsampling and convolution layers, without skip connections. All encoder layers remained trainable to allow full fine-tuning. MobileNet, known for its efficient depthwise separable convolutions, offers a lightweight architecture suitable for low-resource environments. Xception, an advanced variation of the Inception family, uses 36 depthwise separable convolution layers and has demonstrated strong performance on large-scale image datasets. These encoder choices enabled efficient and effective modeling for the segmentation-based detection of intracranial hemorrhage.

While the models were trained for binary segmentation (hemorrhagic vs. non-hemorrhagic regions), the segmentation output was further utilized to derive image-level classification. After the pixel-wise probability mask was predicted by the U-Net-based model, a threshold was applied to generate a binary mask. If any pixels exceeded this threshold, indicating the presence of hemorrhagic features, the image was classified as Hemorrhage (label 1). If no such pixels were detected, the image was classified as Normal (label 0). This approach allowed the segmentation model to serve a dual purpose, enabling both localization and classification without requiring a separate classification head.

4. Results

In the process of training and evaluation, the following metrics are utilized to assess model performance. The quantity of true positives (TP), the quantity of false negatives (FN), and the total number of predictions (TP + FN) are given; sensitivity is calculated as TP/(TP + FN). This demonstrates that sensitivity is employed to determine the model's performance; this assessment is made because it is of paramount clinical importance that no cases of ICH are missed.

For specific hemorrhage types, the U-Net model was customized to perform the classification task, and it achieved the following performance metrics:

Table 1. Performance metrics comparison across models and hemorrhage classes.

Metric	Class	U-Net	U-Net + MobileNet	U-Net + Xception
Accuracy	IPH	98%	99%	98%
	IVH	98%	96%	94%
	SDH	97%	82%	97%
Precision	IPH	99%	99%	99%
	IVH	98%	96%	91%
	SDH	95%	77%	98%
Recall	IPH	98%	100%	97%
	IVH	97%	95%	97%
	SDH	99%	92%	97%
F1 Score	IPH	98%	99%	98%
	IVH	98%	96%	94%
	SDH	97%	84%	97%

Intraparenchymal Hemorrhage (IPH) has an accuracy of 0.98, precision of 0.99, recall of 0.98, and an F1 score of 0.98. Intraventricular Hemorrhage (IVH) shows an accuracy of 0.98, precision of 0.98, recall of 0.97, and an F1 score of 0.98. Subdural Hemorrhage (SDH) presents an accuracy of 0.97, precision of 0.95, recall of 0.99, and an F1 score of 0.97. Table 1 summarizes the evaluation results for the model.

Fig. 5 shows the quantitative evaluation of the evaluation set, which is summarized in the confusion matrix, and Fig. 6 shows some heatmap results for different hemorrhage types.

4.1. Interpretation of results

This paper presents a U-Net model for segmenting the ICH in brain CTs, achieving a mean classification accuracy of 97.7%, calculated as the average of the accuracy scores across the three hemorrhage classes on the evaluation set. By demonstrating high pixel-wise and more abstract metrics, the results will appeal to computer scientists interested in imaging and practitioners who could be affected by advancements. The intersection over union, calculated by overlaying model predictions with ground truth lesions, provides a pixel-wise measure of segmentation quality.

The sensitivity and precision of the model, measuring how often lesions are found and healthy regions are not identified as hemorrhages, respectively, range between 0.97–0.99 and 0.95–0.99, respectively. This high sensitivity shows the extensive checking done in a diagnostic sense and will offer more useful information to healthcare providers. The trade-off between sensitivity and precision can be changed by changing the threshold applied to the predicted probabilities to create a decision boundary used in classification. A lower threshold will increase the number of regions predicted as hemorrhaged (i.e., higher sensitivity), with the reverse occurring when applying a higher threshold. A decision threshold of 0.5 would allow predictions on unseen test cases of comparable imaging quality to be treated as highly compatible with those in work, whilst other scans displaying somewhat varied quality would still not affect the overall results. This would assist in adapting the model to new real-world scenarios with different imaging environments, following the steps of the current work objectives.

4.2. Strengths and limitations of the proposed approaches

The proposed model focused on developing and evaluating three scenarios of deep learning models: U-Net, U-Net combined with MobileNet, and U-Net combined with Xception. The objective was to classify three types of intracranial hemorrhages, IPH, IVH, and SDH, with normal images. The models underwent training and testing on labeled datasets, and their performance was evaluated utilizing key parameters such as accuracy, recall, precision, and F1 score. The statistics in Table 1 give a detailed, comprehensive

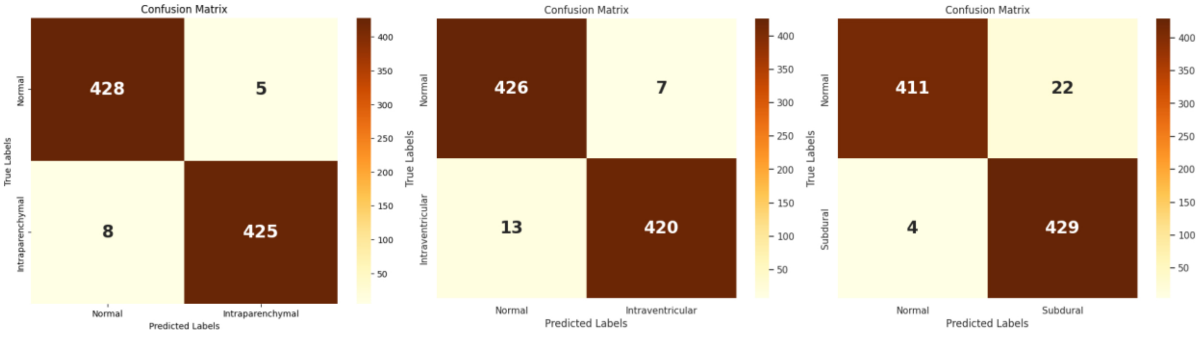

Fig. 5. Confusion matrix (from left to right): Intraparenchymal, intraventricular, subdural.

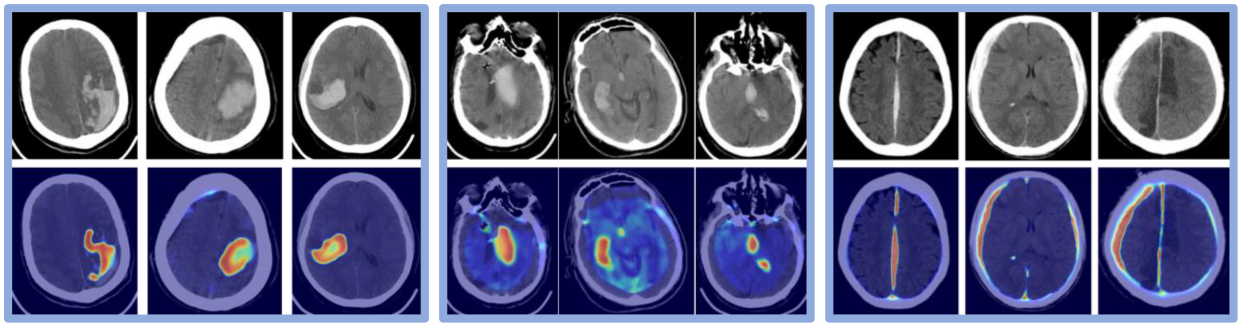

Fig. 6. Heatmap result (From left to right): Intraparenchymal, intraventricular, subdural.

analysis of the models' ability to manage many hemorrhage groups.

In the table, the success measures show how well the U-Net, U-Net with MobileNet, and U-Net with Xception models worked for three types of hemorrhages: intraparenchymal, intraventricular, and subdural. When it comes to accuracy, U-Net combined with MobileNet gets the highest score for IPH (99%), but it scores much lower for SDH (82%), compared to U-Net (97%) and U-Net combined with Xception (97%). These findings show that U-Net with MobileNet performs unevenly across all types of hemorrhage even though it does well in some classes.

For precision, all models perform exceptionally well for IPH, each achieving 99%. However, a significant drop is observed in SDH precision for U-Net with MobileNet (77%) compared to U-Net (95%) and U-Net with Xception (98%), indicating potential challenges in distinguishing SDH when using MobileNet as the backbone.

Regarding recall, U-Net with MobileNet outperforms U-Net and U-Net with Xception for IPH (which shows how well it detects positive instances) but isn't quite up to snuff for IVH and SDH. The dependable nature of these models is featured because the recall for SDH stays high throughout the board, falling anywhere between 92% and 99%.

Last but not least, the F1 Score, which compares accuracy and recall, indicates that U-Net with MobileNet stays competitive for IPH at 99% but falls significantly short for IVH at 96% and SDH at 84%, lagging behind U-Net and U-Net with Xception. While both U-Net and U-Net plus Xception perform admirably across the board, U-Net with Xception just edges out U-Net in terms of SDH recall and precision. According to these data, U-Net and U-Net with Xception give better stability and generalizability across the many types of hemorrhages that were tested, whereas U-Net with MobileNet does show promise for individual instances.

Table 2. Confidence interval summary table.

Model	Class	Accuracy (%)	95% CI Lower (%)	95% CI Upper (%)
U-Net	IPH	98.5	97.69	99.31
	IVH	97.69	96.69	98.69
	SDH	97	95.86	98.13
U-Net + MobileNet	IPH	99.42	98.92	99.93
	IVH	95.61	94.25	96.98
	SDH	82.33	79.79	84.87
U-Net + Xception	IPH	98.04	97.11	98.96
	IVH	93.88	92.28	95.48
	SDH	97.46	96.41	98.51

4.3. Statistical evaluation of model performance

To quantify the statistical reliability of classification performance, confidence intervals (CIs) can be calculated for metrics such as accuracy, precision, and recall. These intervals provide an estimated range within which the true population parameter is likely to lie, with a given level of confidence commonly 95%. When applied to binary outcomes (e.g., correct vs. incorrect prediction), the computation assumes that each prediction represents an independent Bernoulli trial. Under this assumption, the observed accuracy $\hat{p}$ (i.e., the proportion of correct predictions) that follows a binomial distribution. The 95% confidence interval for accuracy can then be approximated using the normal distribution. The results for each model and hemorrhage class are presented in Table 2.

5. Discussion

The presented work utilized deep learning models to classify brain hemorrhages from CT scan images into three categories: intraparenchymal, intraventricular, and subdural, each with normal images. The CT scan relevant information was extracted using deep learning techniques. Earlier studies have enhanced feature extraction and classification accuracy

Table 3. Comparison of the results with the previous model.

Method	Accuracy	Recall
pre-trained ResNet50 2020, Lewicki et al. [26]	IPH 98.5% IVH 99 % SDH 97.8%	76.5% 84.6% 72.2%
pre-trained DenseNet 2023, Arman et al. [29]	IPH 98.5% IVH 98.9% SDH 96.1%	78.2% 82.2% 80.3%
Custom U-Net (proposed model)	IPH 98% IVH 98 % SDH 97%	98% 97% 99%
U-Net with MobileNet (proposed model)	IPH 99% IVH 96 % SDH 82%	100% 95% 92%
U-Net with Xception(proposed model)	IPH 98% IVH 98 % SDH 97%	97% 97% 97%

* All the studies that were compared used part of the RSNA Intracranial Hemorrhage dataset.

using advanced architectures such as ResNet50 and DenseNet. For example, Lewicki et al. used a modified ResNet50 model in 2020 to classify brain hemorrhages using a complete dataset from the RSNA, therefore obtaining a noteworthy accuracy rate [26]. Moreover, Arman et al. developed the DenseNet model through Bayesian optimization to fine-tune hyperparameters, thus improving classification performance, especially in relation to several subtypes of hemorrhage [29]. The current work extracted important imaging characteristics relevant to hemorrhage categorization using U-Net models. Table 3 compares methodologies previously involved in the classification of brain hemorrhages.

Using a transfer learning model as a backbone in U-Net offers advantages such as leveraging pre-trained knowledge for improved feature extraction, faster convergence, and better generalization, especially with small datasets. It also provides robust hierarchical features that enhance segmentation performance. However, it introduces challenges like increased computational cost, potential domain mismatch, risk of overfitting pre-trained features, and reduced interpretability. While ideal for tasks with limited data and sufficient resources, it may not be suitable for large, domain-specific datasets or low-resource environments without careful fine-tuning.

The decision to use a segmentation-based approach followed by image-level classification was made to improve both interpretability and clinical relevance. Unlike direct end-to-end classification models, the segmentation-first approach enables the visualization of hemorrhagic regions, which enhances the transparency of model predictions—an essential factor in medical imaging applications.

6. Conclusion

This work proposed a U-Net-based deep learning model, designed from scratch, for detecting and classifying ICH. The model was compared with two pre-trained transfer learning models, including MobileNet and Xception, used as backbones for the U-Net topology. The models demonstrated good detection accuracy and were significantly faster than the manual measurement approach. Findings revealed that the proposed U-Net model, with its custom-designed layers, outperformed the transfer learning approaches. An unconventional methodology was adopted by training U-Net models for segmentation tasks and subsequently adjusting them to classify images as normal or hemorrhagic, including various hemorrhage subtypes. Such models hold promise as effective solutions for the resource-constrained clinical environment in Iraq because it is fully automatic, can assist the radiologist by indicating the presence of disease, provide an approximation of the ICH volume, and can address the limitations in medical research, and diagnostic capabilities while assisting radiologists in expediting ICH image analysis. Reducing the time required for interpretation can increase the percentage of patients receiving timely medical care. The proposed methods also have some limitations, as they are assumed to be valid for ICH; it is not the size of the ICH but the presence of the disease that dictates treatment selection and prognosis. Future work is planned to involve external validation using independent datasets from different institutions or imaging protocols to assess the generalizability and robustness of the proposed models in real-world clinical environments. Such validation will be important to confirm the applicability of the model across varying populations, scanner types, and clinical settings. This direction is considered essential for supporting the clinical deployment of AI-assisted ICH detection systems.

Ethical statement

All the authors demonstrate that they have adhered to the accepted ethical standards of a genuine research study.

Funding

No funding source is reported for this study.

Declaration of interest

No conflict of interest is declared by the authors.

Acknowledgment

None.

Data sharing statement

Data supporting the findings and conclusions are available upon request from the corresponding author.

References

1. J.-B. Bouillon-Minois *et al.*, "Tranexamic acid in non-traumatic intracranial bleeding: A systematic review and meta-analysis," *Sci Rep*, vol. 11, no. 1, pp. 15275, Jul. 2021, doi: 10.1038/s41598-021-94727-y.
2. E. Wu, S. Marthi, and W. F. Asaad, "Predictors of mortality in traumatic intracranial hemorrhage: A national trauma data bank study," *Front Neurol*, vol. 11, Nov. 2020, doi: 10.3389/fneur.2020.587587.
3. K. de Wit, Z. Merali, Y. K. Kagoma, and É. Mercier, "Incidence of intracranial bleeding in seniors presenting to the emergency department after a fall: A systematic review," *Injury*, vol. 51, no. 2, pp. 157–163, Feb. 2020, doi: 10.1016/j.injury.2019.12.036.
4. C.-Y. Chen *et al.*, "Etiology and risk factors of intracranial hemorrhage and ischemic stroke in young adults," *Journal of the Chinese Medical Association*, vol. 84, no. 10, pp. 930–936, Oct. 2021, doi: 10.1097/JCMA.0000000000000598.
5. A. Alsalihi, H. K. Aljobouri, and E. A. K. ALTameemi, "GLCM and CNN deep learning model for improved MRI breast tumors detection," *International Journal of Online and Biomedical Engineering (iJOE)*, vol. 18, no. 12, pp. 123–137, Sep. 2022, doi: 10.3991/ijoe.v18i12.31897.
6. J. Y. R. Al-Awadi, H. K. Aljobouri, and A. M. Hasan, "MRI brain scans classification using extreme learning machine on LBP and GLCM," *International Journal of Online and Biomedical Engineering (iJOE)*, vol. 19, no. 02, pp. 134–149, Feb. 2023, doi: 10.3991/ijoe.v19i02.33987.
7. K. Malhotra *et al.*, "Prevalence, characteristics, and outcomes of undetermined intracerebral hemorrhage: A systematic review and meta-analysis," *Stroke*, vol. 52, no. 11, pp. 3602–3612, Nov. 2021, doi: 10.1161/STROKEAHA.120.031471.
8. S. M. Mäenpää and M. Korja, "Diagnostic test accuracy of externally validated convolutional neural network (CNN) artificial intelligence (AI) models for emergency head CT scans – A systematic review," *Int J Med Inform*, vol. 189, pp. 105523, Sep. 2024, doi: 10.1016/j.ijmedinf.2024.105523.
9. M. Ivanenko, D. Wanta, W. T. Smolik, P. Wróblewski, and M. Midura, "Generative-adversarial-network-based image reconstruction for the capacitively coupled electrical impedance tomography of stroke," *Life*, vol. 14, no. 3, pp. 419, Mar. 2024, doi: 10.3390/life14030419.
10. H. K. Aljobouri, "Independent component analysis with functional neuroscience data analysis," *J Biomed Phys Eng*, vol. 13, no. 2, Apr. 2023, doi: 10.31661/jbpe.v0i0.2111-1436.
11. S. M. Alnedawe and H. K. Aljobouri, "A new model design for combating COVID -19 pandemic based on SVM and CNN approaches," *Volume 20, Issue 4, Pages 1402 - 1413*, vol. 20, no. 4, pp. 1402–1413, 2023, doi: 10.21123/bsj.2023.7403.
12. A. Petrov *et al.*, "AI-based approach to one-click chronic subdural hematoma segmentation using computed tomography images," *Sensors*, vol. 24, no. 3, pp. 721, Jan. 2024, doi: 10.3390/s24030721.
13. V. V. *et al.*, "Automated detection and screening of Traumatic Brain Injury (TBI) using computed tomography images: A comprehensive review and future perspectives," *Int J Environ Res Public Health*, vol. 18, no. 12, pp. 6499, Jun. 2021, doi: 10.3390/ijerph18126499.
14. Z. Szentimrey, S. de Ribaupierre, A. Fenster, and E. Ukwatta, "Automated 3D U-net based segmentation of neonatal cerebral ventricles from 3D ultrasound images," *Med Phys*, vol. 49, no. 2, pp. 1034–1046, Feb. 2022, doi: 10.1002/mp.15432.
15. C.-Y. Lu *et al.*, "Artificial intelligence application in skull bone fracture with segmentation approach," *Journal of Imaging Informatics in Medicine*, Jul. 2024, doi: 10.1007/s10278-024-01156-0.
16. H. Alrubaie, H. K. Aljobouri, Z. J. AL-Jobawi, and I. Çankaya, "Convolutional neural network deep learning model for improved ultrasound breast tumor classification," *Al-Nahrain Journal for Engineering Sciences*, vol. 26, no. 2, pp. 57–62, Jul. 2023, doi: 10.29194/NJES.26020057.
17. M. A. Probst *et al.*, "Prevalence of intracranial injury in adult patients with blunt head trauma with and without anticoagulant or antiplatelet use," *Ann Emerg Med*, vol. 75, no. 3, pp. 354–364, Mar. 2020, doi: 10.1016/j.annemergmed.2019.10.004.
18. A. Lampart, T. Kuster, C. H. Nickel, R. Bingisser, and V. Pedersen, "Prevalence and severity of traumatic intracranial hemorrhage in older adults with low-energy falls," *J Am Geriatr Soc*, vol. 68, no. 5, pp. 977–982, May 2020, doi: 10.1111/jgs.16400.
19. A. A. Almindelawy and M. H. Ali, "Improvement of eye tracking based on deep learning model for general purpose applications," *Al-Nahrain Journal for Engineering Sciences*, vol. 25, no. 1, pp. 13–19, Apr. 2022, doi: 10.29194/NJES.25010012.
20. R. K. Hamad, "Integrating machine learning and genetic algorithms to enhance gene-disease classification: An XBNet-based framework," *Babylonian Journal of Machine Learning*, vol. 2025, pp. 1–12, Jan. 2025, doi: 10.58496/BJML/2025/001.
21. A. Durairaj, E. S. Madhan, M. Rajkumar, and S. Shameem, "Optimizing anomaly detection in 3D MRI scans: The role of ConvLSTM in medical image analysis," *Appl Soft Comput*, vol. 164, pp. 111919, Oct. 2024, doi: 10.1016/j.asoc.2024.111919.
22. N. Hastings *et al.*, "The role of artificial intelligence-powered imaging in cerebrovascular accident detection," *Cureus*, May 2024, doi: 10.7759/cureus.59768.
23. R. S. Shahadh and B. Al-Khateeb, "Double Dual Convolutional Neural Network (D2CNN): A deep learning model based on feature extraction for skin cancer classification," *Iraqi Journal for Computer Science and Mathematics*, vol. 6, no. 1, Mar. 2025, doi: 10.52866/2788-7421.1240.
24. I. F. Jassam, A. A. Mukhlif, A. A. Nafea, M. A. Tharthar, and A. I. Khudhair, "A review of breast cancer histological image classification: Challenges and limitations," *Iraqi Journal for Computer Science and Mathematics*, vol. 6, no. 1, Feb. 2025, doi: 10.52866/2788-7421.1232.
25. D. Guo *et al.*, "Simultaneous classification and segmentation of intracranial hemorrhage using a fully convolutional neural network," in *Proceedings - International Symposium on Biomed-*

ical Imaging, IEEE Computer Society, pp. 118–121, Apr. 2020, doi: 10.1109/ISBI45749.2020.9098596.

26. T. Lewicki, M. Kumar, R. Hong, and W. Wu, "Intracranial hemorrhage detection in CT scans using deep learning," in *Proceedings - 2020 IEEE 6th International Conference on Big Data Computing Service and Applications, BigDataService 2020*, Institute of Electrical and Electronics Engineers Inc., pp. 169–172, Aug. 2020, doi: 10.1109/BigDataService49289.2020.00033.
27. R. A. Rava *et al.*, "Assessment of an artificial intelligence algorithm for detection of intracranial hemorrhage," *World Neurosurg*, vol. 150, pp. e209–e217, Jun. 2021, doi: 10.1016/j.wneu.2021.02.134.
28. X. Wang *et al.*, "A deep learning algorithm for automatic detection and classification of acute intracranial hemorrhages in head CT scans," *Neuroimage Clin*, vol. 32, Jan. 2021, doi: 10.1016/j.nicl.2021.102785.
29. S. E. Arman *et al.*, "Intracranial hemorrhage classification from CT scan using deep learning and bayesian optimization," *IEEE Access*, vol. 11, pp. 83446–83460, 2023, doi: 10.1109/ACCESS.2023.3300771.
30. "Kaggle and RSNA, 'Intracranial hemorrhage detection dataset,'" [online]. Accessed: Sep. 12, 2024. [Online]. Available: https://www.kaggle.com/c/rsna-intracranialhemorrhage-detection/data.